Thermodynamic assessment of the quaternary Cr–Fe–H–Zr system

Tuan-Minh Vu, Caroline Toffolon-Masclet, Jean-Marc Joubert

Thermodynamic assessment of the quaternary Cr–Fe–H–Zr system

Tuan-Minh Vu[1,2], Caroline Toffolon-Masclet[3] and Jean-Marc Joubert[2]

[1] Université Paris-Saclay, CEA, Service de Recherche en Matériaux et Procédés Avancés, 91191 Gif Sur Yvette, France

[2] Univ. Paris Est Créteil, CNRS, ICMPE, UMR 7182, 2 rue Henri Dunant, 94320 Thiais, France

[3] Université Paris-Saclay, CEA, Service de Recherche en Corrosion et Comportement des Matériaux, 91191 Gif Sur Yvette, France

Abstract

The thermodynamic assessments of the two ternary Cr–H–Zr and Fe–H–Zr systems are carried out using the CALPHAD approach. The hydrogenation properties of all the intermetallic compounds of these two systems are assessed. The formation enthalpies of the $E1_a$-Zr_3FeH_7 and $C16$-Zr_2FeH_5 hydrides are evaluated by DFT calculations. The Pressure-Composition-Temperature diagrams of the $Zr(Cr_xFe_{1-x})_2$ ($0.4 < x < 1.1$) of the $C14$ Laves phase are optimized. The calculations and optimization are carried out under para-equilibrium conditions in which the complete system was treated like a pseudo-binary system.

Keywords: CALPHAD, DFT calculations, Hydrogenation, Para-equilibrium

Introduction

Zirconium-based alloys are used as a material for the fuel claddings in pressurized water reactors thanks to their thermal, mechanical resistance and their low neutron absorption coefficient. During in-service lifetime and/or hypothetical accidental scenario like Loss Of Coolant Accidents (LOCA) of the fuel claddings, it is essential to apprehend and predict

microstructural evolutions. As a result, a thermodynamic database containing all the elements of the fuel claddings Cr, Fe, Nb, Sn, Zr and O is being built by the CALPHAD approach [1,2]. At last, H is also included in order to take into account hydrogenation phenomena.

In literature [1–8], it was reported that hydrides could be formed from the different Cr–Fe–Zr intermetallic compounds. Thus, thermodynamic modeling of two ternary Cr–H–Zr and Fe–H–Zr systems appears to be essential for the thermodynamic database.

To the best of our knowledge, the thermodynamic modeling of the ternary Fe–H–Zr and Cr–H–Zr systems has not been undertaken. A detailed bibliography review of these ternary systems is presented. For the Laves $C14$ phase, the Pressure-Composition-Temperature (P-C-T) diagrams and hydrogenation properties are calculated within para-equilibrium using a pseudo-binary system to constrain the metallic atom ratio. At last, the assessments integrate the hydride formation enthalpies calculated by DFT.

1 Literature survey

1.1 Ternary Fe–H–Zr system

Several authors [9–14] found that Zr_2Fe compound ($C16$ structure, space group $I4/mcm$) can absorb up to 5 H/f.u. Neutron diffraction measurements indicate that the Zr_4 and Zr_3Fe tetrahedral sites are prefered. The hydrogen capacity varies as a function of the temperature. During dehydrogenation, a distortion in the structure, responsible for a space group change from $P4/ncc$ to $I4/mmm$, was observed [10–14]. P-C-T diagrams from 200 to 500 °C are reported by Nobile *et al.* [14]. However, impurities were observed in the compound prior to hydrogenation. First-principles calculations on this hydride were carried out by Chattaraj *et*

al. [15]. The thermodynamic properties including the heat capacity (Cp and Cv) of the hydride were reported.

The intermetallic $ZrFe_2$, which crystallizes with the Laves $C15$ structure, was reported to absorb up to 4 H/f.u at room temperature and very high pressure [8]. Because the Laves $C15$ phase possesses a non-stochiometric domain extending until a composition of $ZrFe_{2.7}$, the P-C-T diagram of $ZrFe_{1.9}$, $ZrFe_{2.0}$ and $ZrFe_{2.5}$ compositions were studied by Zotov *et al.* [16] and Sivov *et al.* [17].

A study conducted by Yartys *et al.* [11,12] focused on the hydride phase formed by the Zr_3Fe intermetallic compound ($E1a$ structure). The hydrogen absorption was reported to be up to 6.7 H/f.u. By neutron diffraction, the hydrogen atoms are reported to occupy the Zr_4, Zr_3Fe and Zr_3Fe_2 interstitial sites.

1.2 Ternary Cr–H–Zr system

In the Cr–Zr binary phase diagram, the intermetallic $ZrCr_2$ compound crystallizes with 3 different polymorphs. The cubic Laves $C15$ structure is stable at low temperatures, it transforms into the hexagonal Laves $C36$ at 1772 K, and the hexagonal Laves $C14$ is stable at high temperatures.

The P-C-T diagram of the Laves $C15$ phase was measured by Krupenchenko *et al.* [3], Andreev *et al.* [4] and Bodega *et al.* [5]. This compound can absorb 4 H/f.u at low pressures. The heat capacity of the Laves $C15$ type $ZrCr_2H_x$ ($0 \leq x \leq 0.5$) in the temperature range 5.3 - 293 K was measured by Skripov *et al.* [18]. An anomaly peak attributed to H ordering was observed. However, due to the limitation of the model used, the experimental measurement of the heat capacity at low temperatures ($T < 200$ K) can not be taken into account.

In the study conducted by Pebler and Gulbransen [7], a P-C-T diagram of $C14$-$ZrCr_2$ was reported. It was found that the hydrogen capacity was only 1.2 H/f.u. However, the measurement was carried out at high temperature and the pressure was limited to 1 bar.

Jacob *et al.* [19] reported that this intermetallic compound can absorb up to 4.5 H/f.u. Hirosawa *et al.* [20] and Skripov *et al.* [6] found that the hexagonal compound can reach a hydrogen content of 4.2 H/f.u. Bodega *et al.* [5] measured the P-C-T diagram of this compound in the temperature range of 348-423 K. It should be noted that their samples contained both Laves $C14$ and Laves $C36$ structures, making the quantification measurement challenging due to overlapping principal peaks on the XRD diffractogram. However, the Laves $C14$ structure was reported to be a major phase and no major difference is expected between the hydrogenation properties of the $C14$ and $C36$ phases, thus the measured data will be considered for the Laves $C14$ phase in our assessment.

To the best of our knowledge, no data was found in the literature concerning hydrogen solubility in α and β-Zr(Cr,Fe) solid solutions.

1.3 Hydrogenation of $Zr(Cr_xFe_{1-x})_2$ compound

Since the $C14$-$ZrCr_2$ compound can absorb hydrogen at low pressures, the substitution of Cr by Fe is promising for hydrogen storage due to its ability to increase the pressure plateau at atmospheric pressure and room temperature. Numerous studies have investigated the hydrides formed from the $Zr(Cr_xFe_{1-x})_2$ compound (x = 0.2 to 0.55). Both the host alloys and the hydrides adopt the Laves $C14$ structure. It has been reported that this compound exhibits hydrogen capacities similar to $C14$-$ZrCr_2$ (3.5 H/f.u) and demonstrates rapid absorption and desorption kinetics. Indeed, the crystal structure of the $C14$-$ZrCr_2$ compound possesses 3

sites: 4*f* occupied by Zr and 2*a*, 6*h* occupied by Cr. The synthesis of *C*14-Zr(Cr_xFe_{1-x})$_2$ compound is carried out by substituting the Cr in 2*a* and 6*h* sites with Fe. Canet *et al.* [21] and Soubeyroux *et al.* [22] reported the site occupancy of these substituted compounds (Figure 1). The occupations of each atom in both sites are equal.

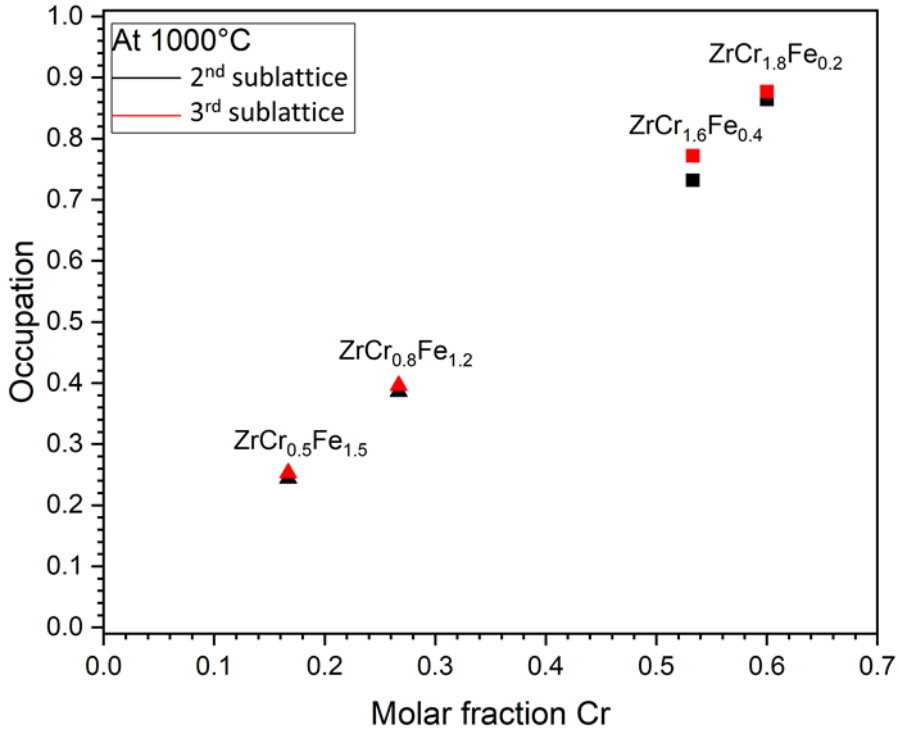

Figure 1: Site occupation of Cr in C14-Zr(Cr_xFe_{1-x})$_2$ structure at 1000°C. △ Canet et al. [21] and ▫ Soubeyroux et al. [22].

Several P-C-T diagrams at different compositions have been reported. Yu *et al.* [23] presented a P-C-T diagram for the *C*14-Zr($Cr_{0.5}Fe_{0.5}$)$_2$ composition at temperatures of 51, 101, and 152 °C. Ivey and Northwood [24,25] measured the P-C-T diagram at 20 °C for the *C*14-Zr($Cr_{0.2}Fe_{0.8}$)$_2$, *C*14-Zr($Cr_{0.25}Fe_{0.75}$)$_2$, and *C*14-Zr($Cr_{0.55}Fe_{0.45}$)$_2$ compositions. Wallace *et al.* [26] reported a P-C-T diagram extending from 23 to 100 °C for the *C*14-Zr($Cr_{0.3}Fe_{0.7}$)$_2$ composition. Zhang and Wallace [27] provided a P-C-T diagram for the *C*14-ZrCrFe composition. Qian and Northwood [28,29] measured the P-C-T diagram for the *C*14-Zr($Cr_{0.2}Fe_{0.8}$)$_2$, *C*14-Zr($Cr_{0.3}Fe_{0.7}$)$_2$, *C*14-Zr($Cr_{0.4}Fe_{0.6}$)$_2$, and *C*14-Zr($Cr_{0.5}Fe_{0.5}$)$_2$

compositions. Park and Lee [30] reported a P-C-T diagram for the $C14$-$ZrCr_{1-y}Fe_{1+y}$ compositions with y values of 0.2, 0.3, and 0.5. Additionally, Grant *et al.* [31] reported a P-C-T diagram for the $C14$-$Zr(Cr_{0.25}Fe_{0.75})_2$ composition.

2 Methodology

2.1 DFT calculations

DFT calculations were carried out to determine the formation enthalpies of the $C16$-Zr_2FeH_5 and $E1a$-Zr_3FeH_7 compounds since they have ordered structures with the atomic positions reported. The calculations were carried out using the Vienna Ab-Initio Simulation (VASP). The Generalized Gradient Approximation (GGA) with the projector augmented wave (PAW) pseudo-potentials of 600 eV were used. The formation enthalpies of the other stable compounds in the system were also calculated to draw a stability envelope of the Fe–H–Zr system. A dense grid of K-points in the Brillouin zone was optimized and used with 11×11×7 k-points meshing for $E1a$-$FeZr_3$ phase, 9×9×9 k-points meshing the Fe_2Zr phase, 5×5×3 k-points meshing the γZrH phase, 7×7×7 k-points meshing the δZrH_{2-x} phase, 11×11×11 k-points meshing the ϵZrH_2 phase, 9×11×11 k-points meshing the $C16$-Zr_2FeH_5 phase and 9×9×5 k-points meshing the $E1a$-Zr_3FeH_7 phase.

The formation enthalpy is obtained by subtracting the DFT total energy of the calculated structure to the molar fraction weighted sum of the DFT energies of the pure elements in their Stable Element Reference (SER), i.e., ground-state structure for Fe (magnetic) in bcc, Zr in hcp and H in gas.

2.2 The CALPHAD method

The CALPHAD method involves the optimization of the Gibbs energy for each phase in the system in order to match the available experimental data. The Gibbs energies are represented by equations that contain adjustable parameters. Through this assessment, phase equilibria and thermodynamic properties that have not been studied experimentally can be predicted. Detailed information about the CALPHAD method can be found in the Lukas *et al.* [32] textbook.

Thermodynamic modelling

2.2.1 Gas phase

Since the hydrides are formed at an intermediate pressure (below 100 bar), the gas phase has been considered as ideal. The Gibbs energy of the H_2 species in its stable-element reference (SER) state at a temperature of 298.15 K and pressure of 10^5 Pa is obtained from the PURE database.

The Gibbs energy of pure hydrogen can be represented as:

$$G^{gas} = G_{H_2}^{SER} + RTln(P/P_0)$$

2.2.2 Solid phases

The Gibbs energy function of pure elements is taken in the PURE database. Since the crystal structures do not change before and after hydrogenation, the distorsion observed in $C16$ $-Zr_2Fe$ hydride is not considered, the hydride phases are treated as solid solutions. Taking the example of the $C15$-$Zr(Cr_xFe_{1-x})_2H_4$ hydride, the compound is modeled with 4 sublattices corresponding to 4 cristal sites: $(Zr)_4(Cr_{y_{Cr}^{(2)}}Fe_{y_{Fe}^{(2)}})_2(Cr_{y_{Cr}^{(3)}}Fe_{y_{Fe}^{(3)}})_6(H,Va)_{14}$. The occupation fraction of A element (A = Cr or Fe) in the b (b = 2 or 3) sublattice is written $y_A^{(b)}$ in the hydride composition. The thermodynamic modeling of the Cr–Fe–Zr system was

defined by Lafaye [1]. The end-member energies and interaction parameters of intermetallic compounds from [1] will not be modified in this study. Three end-members $G^{Laves\_C14}_{Zr:Cr:Cr:Va}, G^{Laves\_C14}_{Zr:Fe:Fe:Va}, G^{Laves\_C14}_{Zr:Cr:Fe:Va}, G^{Laves\_C14}_{Zr:Fe:Cr:Va}$ and four interaction parameters ${}^0L^{Laves\_C14}_{Zr:Cr,Fe:Cr:Va}, {}^0L^{Laves\_C14}_{Zr:Cr,Fe:Fe:Va}, {}^0L^{Laves\_C14}_{Zr:Cr,Fe:Cr,Fe:Va}$ were optimized. The Gibbs energy of this compound can be expressed as:

$$G^{Laves\_C14} = {}^{ref}G^{Laves\_C14} + {}^{id}G^{Laves\_C14} + {}^{ex}G^{Laves\_C14} \quad \#(1)$$

Where

$$\begin{aligned} {}^{ref}G^{Laves\_C14} = {} & y^{(2)}_{Cr}y^{(3)}_{Cr}y_{Va}G^{Laves\_C14}_{Zr:Cr:Cr:Va} + y^{(2)}_{Fe}y^{(3)}_{Fe}y_{Va}G^{Laves\_C14}_{Zr:Fe:Fe:Va} + y^{(2)}_{Cr}y^{(3)}_{Fe}y_{Va}G^{Laves\_C14}_{Zr:Cr:Fe:Va} \\ & + y^{(2)}_{Fe}y^{(3)}_{Cr}y_{Va}y_{Va}G^{Laves\_C14}_{Zr:Fe:Cr:Va} + y^{(2)}_{Cr}y^{(3)}_{Cr}y_{H}G^{Laves\_C14}_{Zr:Cr:Cr:H} + y^{(2)}_{Fe}y^{(3)}_{Fe}y_{H}G^{Laves\_C14}_{Zr:Fe:Fe:H} \\ & + y^{(2)}_{Cr}y^{(3)}_{Fe}y_{H}G^{Laves\_C14}_{Zr:Cr:Fe:H} + y^{(2)}_{Fe}y^{(3)}_{Cr}y_{H}G^{Laves\_C14}_{Zr:Fe:Cr:H} \quad \#(2) \end{aligned}$$

$$\begin{aligned} {}^{id}G^{Laves\_C14} = {} & 2RT\left(y^{(2)}_{Cr}lny^{(2)}_{Cr} + y^{(2)}_{Fe}lny^{(2)}_{Fe}\right) + 6RT\left(y^{(3)}_{Cr}lny^{(3)}_{Cr} + y^{(3)}_{Fe}lny^{(3)}_{Fe}\right) \\ & + 14RT(y_{H}lny_{H} + y_{Va}lny_{Va}) \ \#(3) \end{aligned}$$

$$\begin{aligned} {}^{ex}G^{Laves\_C14} = {} & y^{(2)}_{Cr}y^{(2)}_{Fe}y^{(3)}_{Cr}y_{Va}\ {}^0L^{Laves\_C14}_{Zr:Cr,Fe:Cr:Va} + y^{(2)}_{Cr}y^{(2)}_{Fe}y^{(3)}_{Fe}y_{Va}\ {}^0L^{Laves\_C14}_{Zr:Cr,Fe:Fe:Va} \\ & + y^{(2)}_{Cr}y^{(2)}_{Fe}y^{(3)}_{Cr}y^{(3)}_{Fe}y_{Va}\ {}^0L^{Laves\_C14}_{Zr:Cr,Fe:Cr,Fe:Va} + y^{(2)}_{Cr}y^{(2)}_{Fe}y^{(3)}_{Cr}y_{H}\ {}^0L^{Laves\_C14}_{Zr:Cr,Fe:Cr:H} \\ & + y^{(2)}_{Cr}y^{(2)}_{Fe}y^{(3)}_{Fe}y_{H}\ {}^0L^{Laves\_C14}_{Zr:Cr,Fe:Fe:H} + y^{(2)}_{Cr}y^{(2)}_{Fe}y^{(3)}_{Cr}y^{(3)}_{Fe}y_{H}\ {}^0L^{Laves\_C14}_{Zr:Cr,Fe:Cr,Fe:H} \\ & + y^{(2)}_{Cr}y^{(3)}_{Cr}y_{H}y_{Va}\ {}^0L^{Laves\_C14}_{Zr:Cr:Cr:H,Va} + y^{(2)}_{Fe}y^{(3)}_{Fe}y_{H}y_{Va}\ {}^0L^{Laves\_C14}_{Zr:Fe:Fe:H,Va} \\ & + y^{(2)}_{Fe}y^{(3)}_{Cr}y_{H}y_{Va}\ {}^0L^{Laves\_C14}_{Zr:Fe:Cr:H,Va} + y^{(2)}_{Cr}y^{(3)}_{Fe}y_{H}y_{Va}\ {}^0L^{Laves\_C14}_{Zr:Cr:Fe:H,Va} \\ & + y^{(2)}_{Cr}y^{(3)}_{Cr}y_{H}y_{Va}(y_{H} - y_{Va})\ {}^1L^{Laves\_C14}_{Zr:Cr:Cr:H,Va} \\ & + y^{(2)}_{Fe}y^{(3)}_{Fe}y_{H}y_{Va}(y_{H} - y_{Va})\ {}^1L^{Laves\_C14}_{Zr:Fe:Fe:H,Va} \ \#(4) \end{aligned}$$

The thermodynamic model used to describe the hydride phases formed from intermetallic compounds in the Cr–Fe–H–Zr quaternary system is presented in Table 1:

Table 1. Thermodynamic model of hydride compounds in the Cr–Fe–H–Zr quaternary system

Phase	$C16$	Laves $C15$	Laves $C14$	$E1a$

Model	$(Fe,Zr)(Fe,Zr)_2(H,Va)_5$	$(Cr,Fe,Zr)_2(Cr,Fe,Zr)(H,Va)_4$	$(Cr,Fe,Zr)_4(Cr, Fe,Zr)_2(Cr, Fe,Zr)_6(H,Va)_{16}$	$(Fe,Zr)(Fe,Zr)_3(H,Va)_7$

2.3 Calculation and optimization of the para-equilibrium conditions

Para-equilibrium occurs when there are differences in the diffusion rates of the constituting elements at a given temperature. During the para-equilibrium state, the elements with higher diffusion rates tend to reach equilibrium, while the elements with slower diffusion rates remain relatively stationary. In the specific context of hydrogen storage materials, the measurements are often carried out close to room temperature where the metallic elements can be considered as frozen. This has two consequences. Firstly, hydrides of intermetallic compounds may be observed while the most stable state often corresponds to the decomposition into the hydrides of the pure elements. Secondly, when an equilibrium is observed between an intermetallic compound and its hydride, both have the same metallic compositions.

For the hydrides forming through a continuous solid solution, only the first problem is relevant and can be treated by suspending the other phases in the system to avoid the decomposition. However, for the hydrides forming by a phase transformation, whether because the structures are different or due to the presence of a miscibility gap, the observed para-equilibrium must be treated specifically. An additional constraint to fix the ratios of metallic elements should be introduced.

Pelton *et al.* [33] carried out the calculations in para-equilibrium by using virtual elements to apply a constraint to the composition. Nevertheless, the miscibility gap was not a focal point within their method. Recently, Hannappel et al. [34] made progress in the thermodynamic

modeling of multicomponent phases in para-equilibrium by creating an open-source Python tool that is integrated into the CALPHAD framework.

Joubert and Thiébaut [35] calculated P-C-T diagrams with the presence of the miscibility gap by treating the system as pseudo-binary, i.e. the intermetallic solid solution was treated by a pseudo-binary atom to ensure that the metallic composition remained constant throughout hydrogenation.

The same method is used in this work and explained in the following paragraph.

Hence, a pseudo-atom Z = $(Zr)_4(Cr_{y_{Cr}^{(2)}}Fe_{y_{Fe}^{(2)}})_2(Cr_{y_{Cr}^{(3)}}Fe_{y_{Fe}^{(3)}})_6$ representing the intermetallic part of hydride is introduced (with y_{Cr} and y_{Fe} the site occupation of Cr and Fe respectively). The Gibbs energy for the solid phase in the pseudo-binary system can be written by the functions depending on the parameters in the ternary system:

$$G^{*Laves\_C14} = {}^{ref}G^{*Laves\_C14} + {}^{id}G^{*Laves\_C14} + {}^{ex}G^{*Laves\_C14} \#(5)$$

where

$${}^{ref}G^{*Laves\_C14} = y_{Va}G_{Z:Va}^{Laves\_C14} + y_H G_{Z:H}^{Laves\_C14} \#(6)$$

$${}^{id}G^{*Laves\_C14} = RT(y_H lny_H + y_{Va} lny_{Va}) \#(7)$$

$${}^{ex}G^{*Laves\_C14} = y_H y_{Va} \sum_{v=0}^{n} {}^{v}L_{Z:H,Va}^{Laves\_C14}(y_H - y_{Va})^v \#(8)$$

The equations (1) and (5) have to be identical, the following relationships are given:

$$G_{Z:Va}^{Laves\_C14} = y_{Cr}^{(2)} y_{Cr}^{(3)} G_{Zr:Cr:Cr:Va}^{Laves\_C14} + y_{Fe}^{(2)} y_{Fe}^{(3)} G_{Zr:Fe:Fe:Va}^{Laves\_C14} + y_{Cr}^{(2)} y_{Fe}^{(3)} G_{Zr:Cr:Fe:Va}^{Laves\_C14} + y_{Fe}^{(2)} y_{Cr}^{(3)} G_{Zr:Fe:Cr:Va}^{Laves\_C14} + y_{Cr}^{(2)} y_{Fe}^{(2)} y_{Cr}^{(3)} {}^{0}L_{Zr:Cr,Fe:Cr:Va}^{Laves\_C14} + y_{Cr}^{(2)} y_{Fe}^{(2)} y_{Fe}^{(3)} {}^{0}L_{Zr:Cr,Fe:Fe:Va}^{Laves\_C14} + y_{Cr}^{(2)} y_{Fe}^{(2)} y_{Cr}^{(3)} y_{Fe}^{(3)} {}^{0}L_{Zr:Cr,Fe:Cr,Fe:Va}^{Laves\_C14} + RT\left(y_{Cr}^{(2)} ln y_{Cr}^{(2)} + y_{Fe}^{(2)} ln y_{Fe}^{(2)} + y_{Cr}^{(3)} ln y_{Cr}^{(3)} + y_{Fe}^{(3)} ln y_{Fe}^{(3)}\right) \#(9)$$

$$G_{Z:H}^{Laves\_C14} = y_{Cr}^{(2)} y_{Cr}^{(3)} G_{Zr:Cr:Cr:H}^{Laves\_C14} + y_{Fe}^{(2)} y_{Fe}^{(3)} G_{Zr:Fe:Fe:H}^{Laves\_C14} + y_{Cr}^{(2)} y_{Fe}^{(3)} G_{Zr:Cr:Fe:H}^{Laves\_C14} + y_{Fe}^{(2)} y_{Cr}^{(3)} G_{Zr:Fe:Cr:H}^{Laves\_C14} + y_{Cr}^{(2)} y_{Fe}^{(2)} y_{Cr}^{(3)} {}^{0}L_{Zr:Cr,Fe:Cr:H}^{Laves\_C14} + y_{Cr}^{(2)} y_{Fe}^{(2)} y_{Fe}^{(3)} {}^{0}L_{Zr:Cr,Fe:Fe:H}^{Laves\_C14} + y_{Cr}^{(2)} y_{Fe}^{(2)} y_{Cr}^{(3)} y_{Fe}^{(3)} {}^{0}L_{Zr:Cr,Fe:Cr,Fe:H}^{Laves\_C14} + RT\left(y_{Cr}^{(2)} ln y_{Cr}^{(2)} + y_{Fe}^{(2)} ln y_{Fe}^{(2)} + y_{Cr}^{(3)} ln y_{Cr}^{(3)} + y_{Fe}^{(3)} ln y_{Fe}^{(3)}\right) \#(10)$$

$${}^{0}L_{Z:H,Va}^{Laves\_C14} = y_{Cr}^{(2)} y_{Cr}^{(3)} {}^{0}L_{Zr:Cr:Cr:H,Va}^{Laves\_C14} + y_{Fe}^{(2)} y_{Fe}^{(3)} {}^{0}L_{Zr:Fe:Fe:H,Va}^{Laves\_C14} + y_{Fe}^{(2)} y_{Cr}^{(3)} {}^{0}L_{Zr:Fe:Cr:H,Va}^{Laves\_C14} + y_{Cr}^{(2)} y_{Fe}^{(3)} {}^{0}L_{Zr:Cr:Fe:H,Va}^{Laves\_C14} \#(11)$$

$${}^{1}L_{Z:H,Va}^{Laves\_C14} = y_{Cr}^{(2)} y_{Cr}^{(3)} {}^{1}L_{Zr:Cr:Cr:H,Va}^{Laves\_C14} + y_{Fe}^{(2)} y_{Fe}^{(3)} {}^{1}L_{Zr:Fe:Fe:H,Va}^{Laves\_C14} \#(12)$$

3 Results

3.1 DFT results

The formation enthalpies of the end-members of $E1_a$-Zr_3Fe and $C16$-Zr_2Fe hydrides and stable end-members of binary phases are presented in Table 2. The calculated values in this work are close to the reported values in the literature.

Table 2: DFT calculation results for the Fe–H–Zr system and comparison with experimental values from literature

Space group	Prototype	Configuration	$\Delta_f H$ (this work)	$\Delta_f H$ (in literature)
			(kJ/mol.at)	(kJ/mol.at)
$P4/ncc(130)$ (Distored structure)	Filled Al_2Cu	Zr_2FeH_5	-40.69	-39.20 [15], -37.65 [36]
		$ZrFe_2H_5$	76.42	
		Fe_3H_5	15.25	
		Zr_3H_5	-33.53	

$Cmcm(63)$ ($E1a$)	Filled Re_3B	Zr_3FeH_7	-39.91	-36.14 [36]
		$ZrFe_3H_7$	6.85	
		Fe_4H_7	13.11	
		Zr_4H_7	-29.84	
$I4/mmm(139)$	ThH_2	ϵZrH_2	-55.16	-49.67 [37]
$Fm\bar{3}m(225)$	CaF_2	δZrH_{2-x}	-54.23	-48.3 [37]
$Cccm(66)$	PtS	γZrH	-41.58	-58 [37]
$Fd\bar{3}m(227)$ (Laves C15)	$MgCu_2$	$ZrFe_2$	-28.78	-35.03 [1]
$I4/mcm(140)$	$CuAl_2$	Zr_2Fe	-15.65	-17.35 [1]

The hydride stabilities were checked by drawing the stability envelope (Figure 2). This envelope is drawn by the convex hull algorithm [38]. The vertical axis is the formation enthalpy values of binary and ternary compounds obtained by DFT calculations and the horizontal plane is the composition plane.

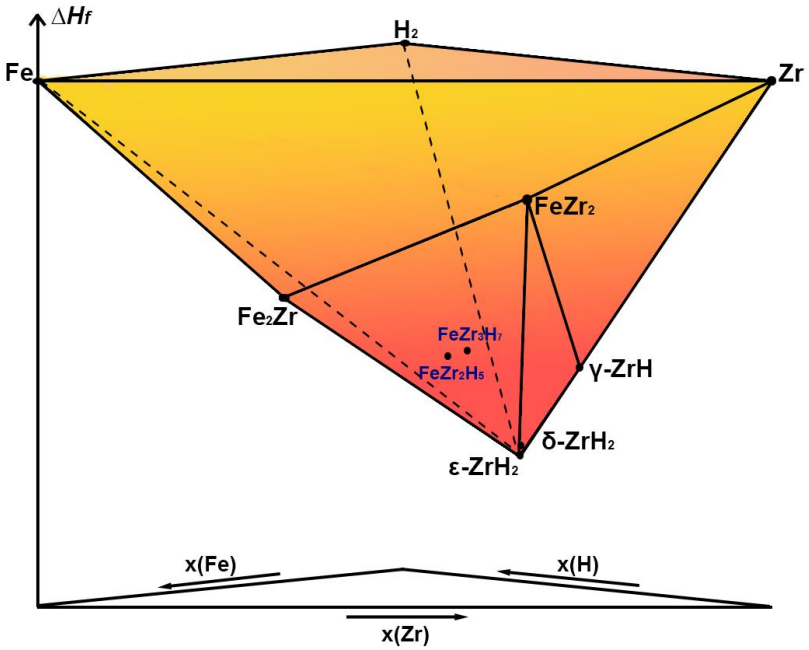

Figure 2: Stability envelope of Fe–H–Zr system

Both ternary hydrides are located above the envelope. The distances between the $E1a$-Zr_3FeH_7 and $C16$-Zr_2FeH_5 to the envelope are 5.06 kJ/mol.at and 0.47 kJ/mol.at respectively. Indeed, these hydrides are metastable. The stable equilibrium for these compositions is the Fe + H_2 + ϵZrH_2 equilibrium.

3.2 Fe–H–Zr system

In order to model the Fe–H–Zr system, three binary systems Fe–Zr, H–Zr and Fe–H are combined using the database of Lafaye [1], Zhong [39] and Zinkevich [40] respectively. The multiplicity of the interstitial sites within the HCP_*A3* phase of the H–Zr system is modified from $(Zr)(H,Va)_1$ to $(Zr)(H,Va)_2$ and the one within the BCC_*A2* phase of the Fe–H system is converted from $(Fe)(H,Va)_1$ to $(Fe)(H,Va)_3$ using Tai's model [41], [42]. The hydrides in this system are modeled as solid solutions. The multiplicity of hydrogen sublattices corresponds to the maximal hydrogen absorption capacity. The enthalpic parameters of all end-members of the hydrides formed from $C16$ and $E1a$ structures are fixed to DFT calculated values. The entropy difference between a solid phase with gas and the hydride is approximatively equal to the entropy of the disappearing gas phase ($\sim$ 130 J.mol^{-1} (H_2)). This approximative value is applied to the entropic parameters of all end-members of hydride phases. In order to optimize the heat capacity of $C16$-Zr_2FeH_5 hydride, supplementary parameters dependent on the temperature are adjusted. The enthalpic parameters of hydrides formed from $Laves\ C15$ $ZrFe_x$ are adjusted to optimize the pressure plateaus of $ZrFe_x$–H (x = 1.9, 2.0 and 2.5) P-C-T diagrams.

Figure 3 represents the hydrogen capacity as a function of the temperature at atmospheric pressure, P-C-T diagram and the heat capacity as a function of the temperature

of the hydride $C16$-Zr_2FeH_5. The calculated lines are in acceptable agreement. However, the gap within the P-C-T diagram is explained by the impurities observed by Nobile *et al.* [14].

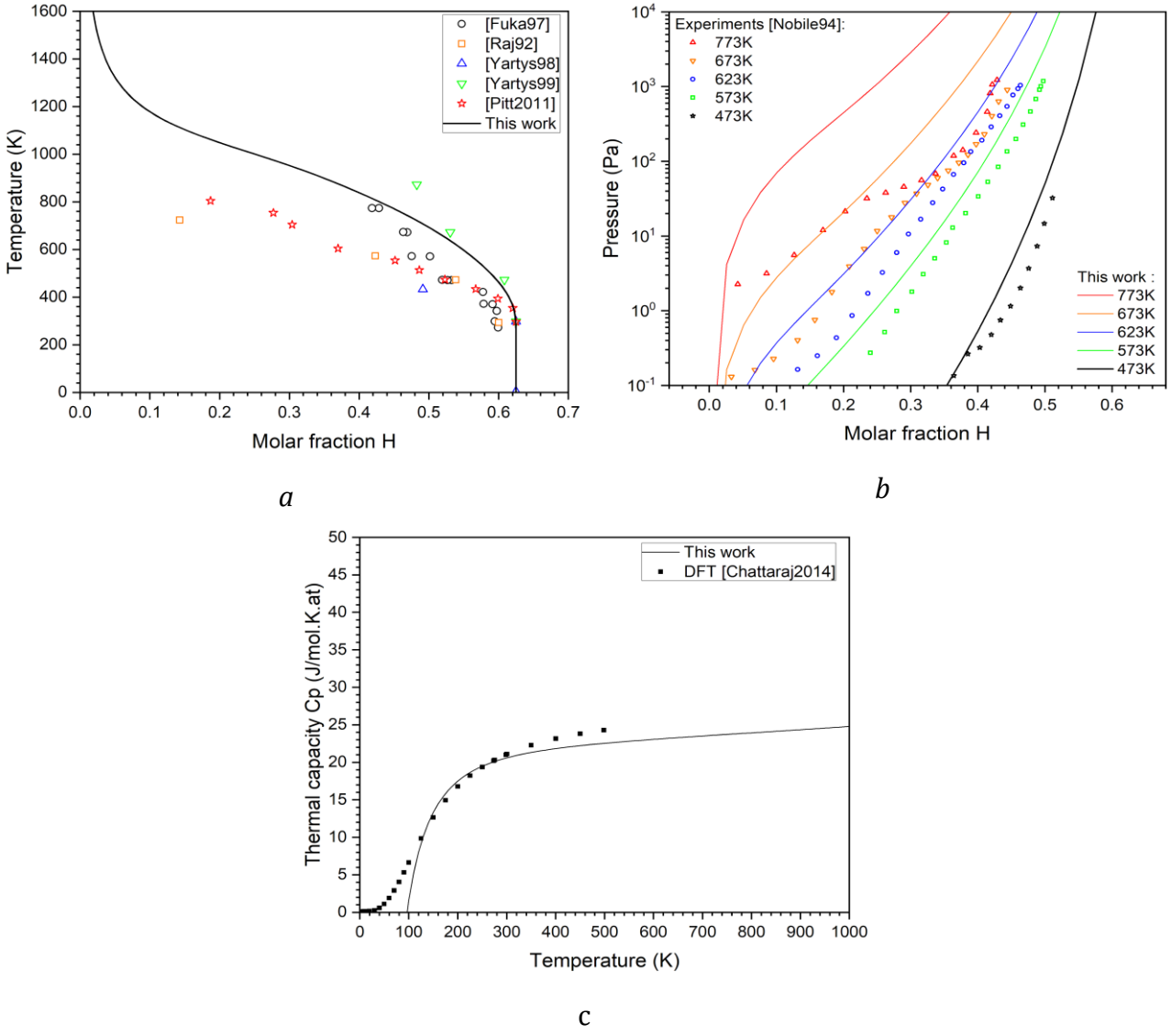

Figure 3: Hydride C16-Zr_2FeH_5: (a) hydrogen capacity as a function of the temperature at ambient pressure [9–13]; (b) P-C-T diagram [14], (c) heat capacity as a function of the temperature [15].

Figure 4 represents the P-C-T diagrams of three compositions $C15$-$ZrFe_{1.9}$-H_x, $C15$-$ZrFe_{2.0}$-H_x and $C15$-$ZrFe_{2.5}$-H_x. The calculated diagrams are in agreement with the experimental points.

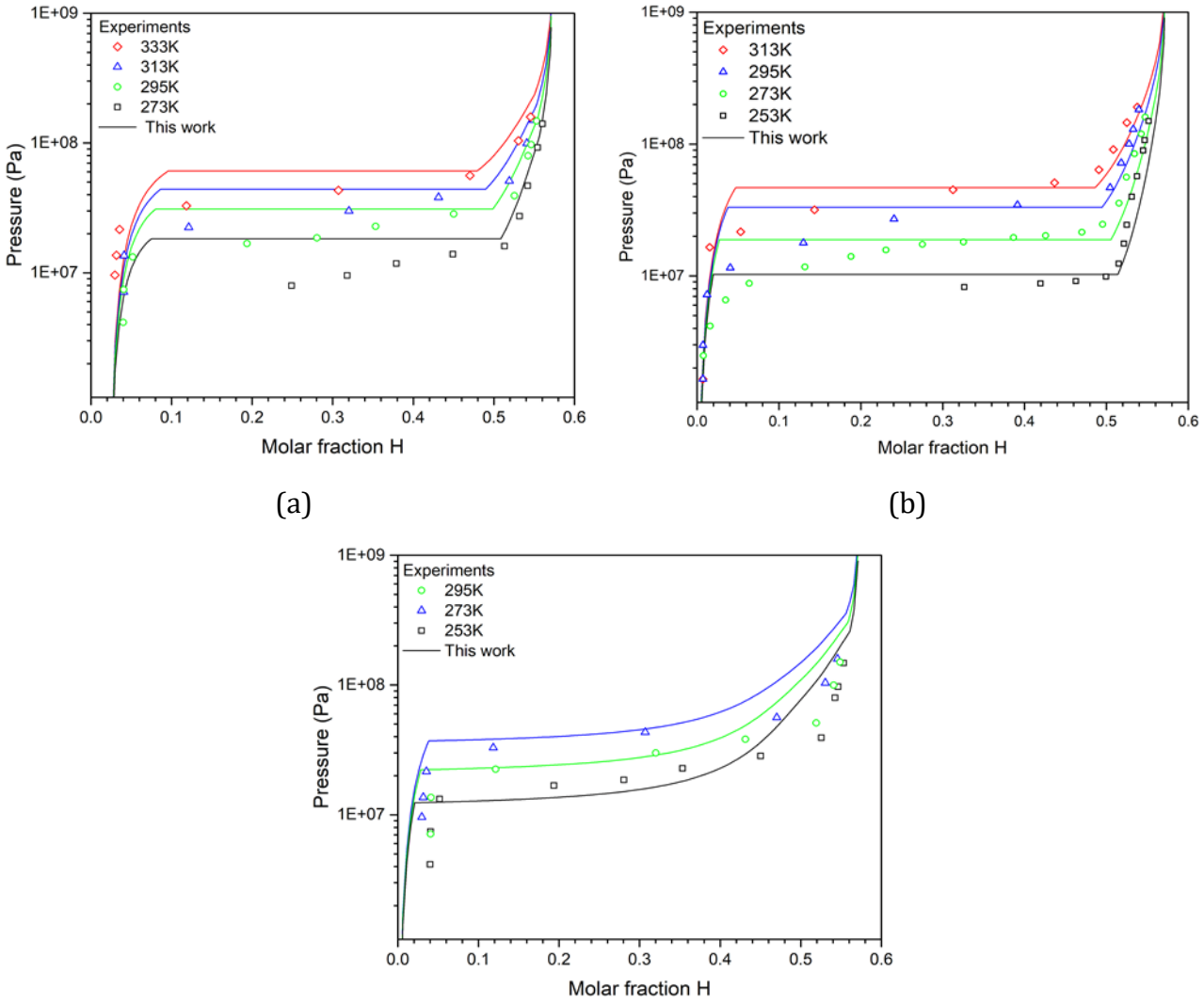

Figure 4: P-C-T diagram of three compositions (a) C15-$ZrFe_{1.9}$–H_x, (b) C15-$ZrFe_{2.0}$–H_x and (c) C15-$ZrFe_{2.5}$–H_x compared to experimental measurements [16,17].

The hydrogen capacity measurement for the $E1a$-Zr_3Fe compound has been effectively implemented (Figure 5a). Finally, Figure 5b presents an isothermal section in full equilibrium at ambient temperature and atmospheric pressure. The three points on the figure are the compositions of three hydrides at their maximal hydrogen content. Indeed, at full equilibrium, these hydrides are unstable compared to the decomposition into Fe, H_2 and ϵZrH_2.

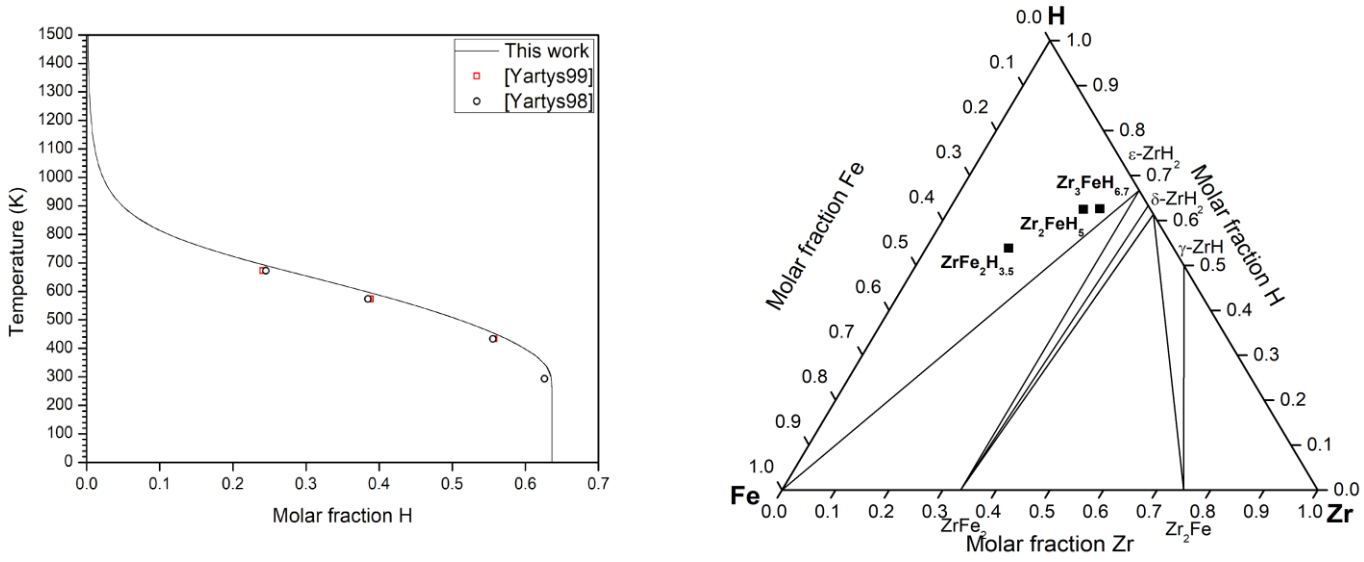

(a) (b)

Figure 5: (a) Hydrogen capacity of the E1a-Zr_3Fe compound as a function of the temperature; (b) isothermal section at 293K in full equilibrium. · represent hydrides at their maximal hydrogen content.

3.3 Cr–H–Zr system

The Cr–Zr, H–Zr and H–Cr databases of Lafaye [1], Zhong [39] and Dottor [43] are utilized to extrapolate the Cr–H–Zr system. Hydrogen is modeled as an interstitial sublattice which multiplicity corresponds to the maximal hydrogen absorption capacity. The entropy of hydride configurations is fixed to the approximative entropy value ($\sim$ 130 J.mol^{-1} (H_2)). The enthalpic parameter of the $G_{Cr:Zr:H}^{Laves\_C15}$ end-member is adjusted to optimize the pressure plateau. The adjustment of the other end-members has been done by comparison with the with the results found in the Fe-H-Zr system. The formation enthalpy difference between the stable end-members $G_{Cr:Zr:H}^{Laves\_C15}$ and $G_{Fe:Zr:H}^{Laves\_C15}$ is $|\Delta H_f| = 12500$ J.mol^{-1} (H), the enthalpic parameters of the two end-members $G_{Fe:Fe:H}^{Laves\_C15}$ and $G_{Zr:Fe:H}^{Laves\_C15}$ are adjusted in order to optimize the pressure plateau of $C15$-$ZrFe_{1,9}H_{3,5}$ and $C15$-$ZrFe_{2,5}H_{3,5}$ hydrids. Finally, the enthalpic parameters of the two end-members $G_{Cr:Cr:H}^{Laves\_C15}$ and $G_{Zr:Cr:H}^{Laves\_C15}$ are estimated from

the values obtained for the two end-members $G_{Fe:Fe:H}^{Laves\_C15}$ and $G_{Zr:Fe:H}^{Laves\_C15}$ applying the difference obtained between $G_{Cr:Zr:H}^{Laves\_C15}$ and $G_{Fe:Zr:H}^{Laves\_C15}$ $G_{Fe:Fe:H}^{Laves\_C15}$ and $G_{Zr:Fe:H}^{Laves\_C15}$. Figure 6 illustrates the formation enthalpies of end-members of the hydrides formed from Laves $C15$ in both Fe–H–Zr and Cr–H–Zr systems.

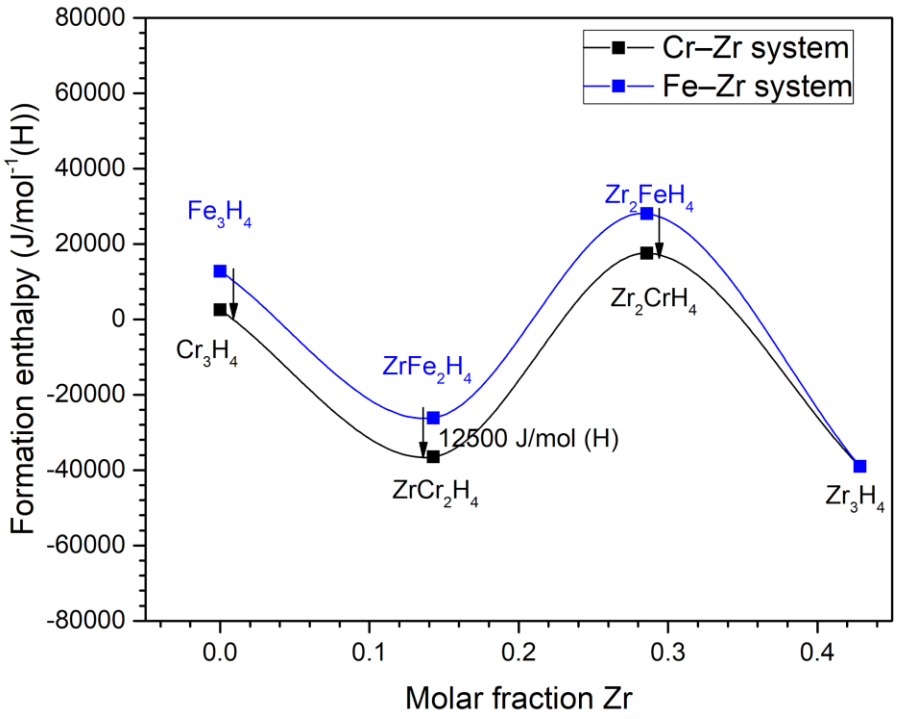

Figure 6: Formation enthalpies of end-members of Laves C15 hydrides in Fe–H–Zr and Cr–H–Zr systems

The calculated P-C-T diagram of the hydrides formed from Laves $C15$ and Laves $C14$ structures in Figure 7 is in agreement with the experimental points. On the P-C-T diagram of Laves $C14$ hydride, the experimental points at high temperatures of Pebler and Gulbransen [7] are optimized with less weight.

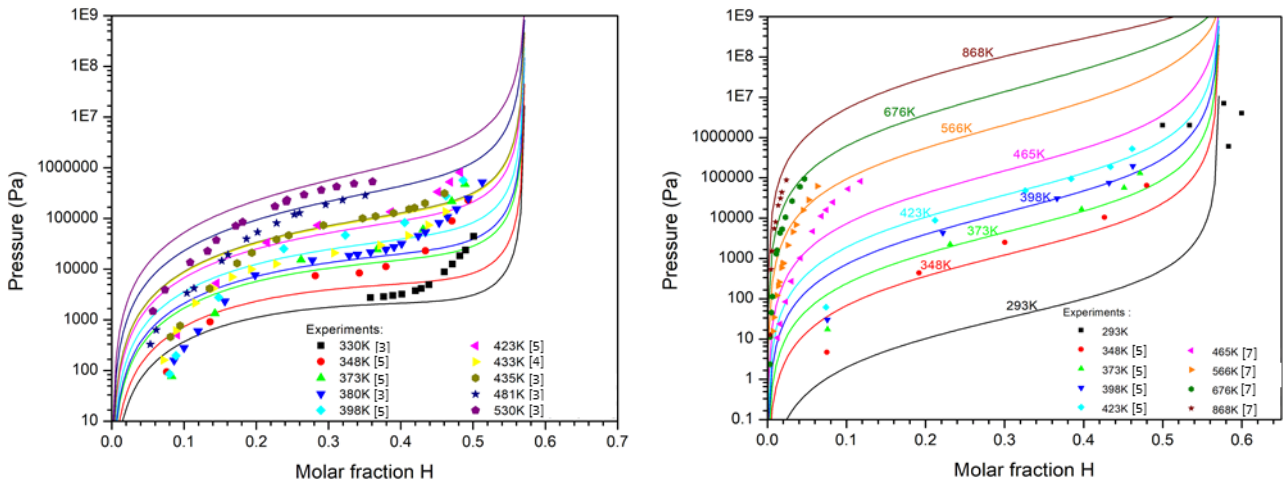

(a) (b)

Figure 7: P-C-T diagrams of hydrides formed from $ZrCr_2$ compound of Laves C15 (a) and Laves C14 (b) structures

3.4 $Zr(Cr_xFe_{1-x})_2$ hydride

In the Cr–H–Zr system, both Laves $C14$ and Laves $C15$ structures exist. The Laves $C15$ structure is predominantly present near the Cr–Zr and Fe–Zr binary systems. The Laves $C14$ phase, on the other hand, is situated at intermediate compositions between $ZrCr_2$ and $ZrFe_2$. The hydrogen capacity of these structures is similar (3.5 H/f.u) and their plateau pressure values at the same temperature are close. Therefore, the thermodynamic properties of the hydrides formed from this composition are similar for both structures. In the same way, the $G_{Zr:Fe:Fe:H}^{Laves\_C14}$ and $G_{Fe:Zr:H}^{Laves\_C15}$ parameters give the same composition: $ZrFe_2H_4$ in both structures. The enthalpic and entropic parameters of these end-members should be approximatively equal. The enthalpic and entropic parameters of three end-members $G_{Zr:Fe:Fe:H}^{Laves\_C14}$, $G_{Zr:Fe:Cr:H}^{Laves\_C14}$ and $G_{Zr:Cr:Fe:H}^{Laves\_C14}$ are adjusted to optimize the pressure plateau of the entire composition range $Zr(Cr_xFe_{1-x})_2$. Regarding the metallic atom interaction parameters for hydrides, as the

metallic composition of the hydrides remains unchanged compared to the intermetallic compounds, these parameters are set to be identical to those of the intermetallic compounds:

${}^{0}L^{Laves\_C14}_{Zr:Cr,Fe:Cr:Va} = {}^{0}L^{Laves\_C14}_{Zr:Cr,Fe:Cr:H}$ ${}^{0}L^{Laves\_C14}_{Zr:Cr,Fe:Fe:Va} = {}^{0}L^{Laves\_C14}_{Zr:Cr,Fe:Fe:H}$ ${}^{0}L^{Laves\_C14}_{Zr:Cr,Fe:Cr,Fe:Va} = {}^{0}L^{Laves\_C14}_{Zr:Cr,Fe:Cr,Fe:H}$

The interaction parameters ${}^{0}L^{Laves\_C14}_{Zr:Fe:Cr:H,Va}$ and ${}^{0}L^{Laves\_C14}_{Zr:Cr:Fe:H,Va}$ are adjusted. The interaction parameters ${}^{0}L^{Laves\_C14}_{Zr:Fe:Fe:H,Va}$ and ${}^{1}L^{Laves\_C14}_{Zr:Fe:Fe:H,Va}$ are approximately equal to the interaction parameters ${}^{0}L^{Laves\_C15}_{Fe:Zr:H,Va}$ and ${}^{1}L^{Laves\_C15}_{Fe:Zr:H,Va}$.

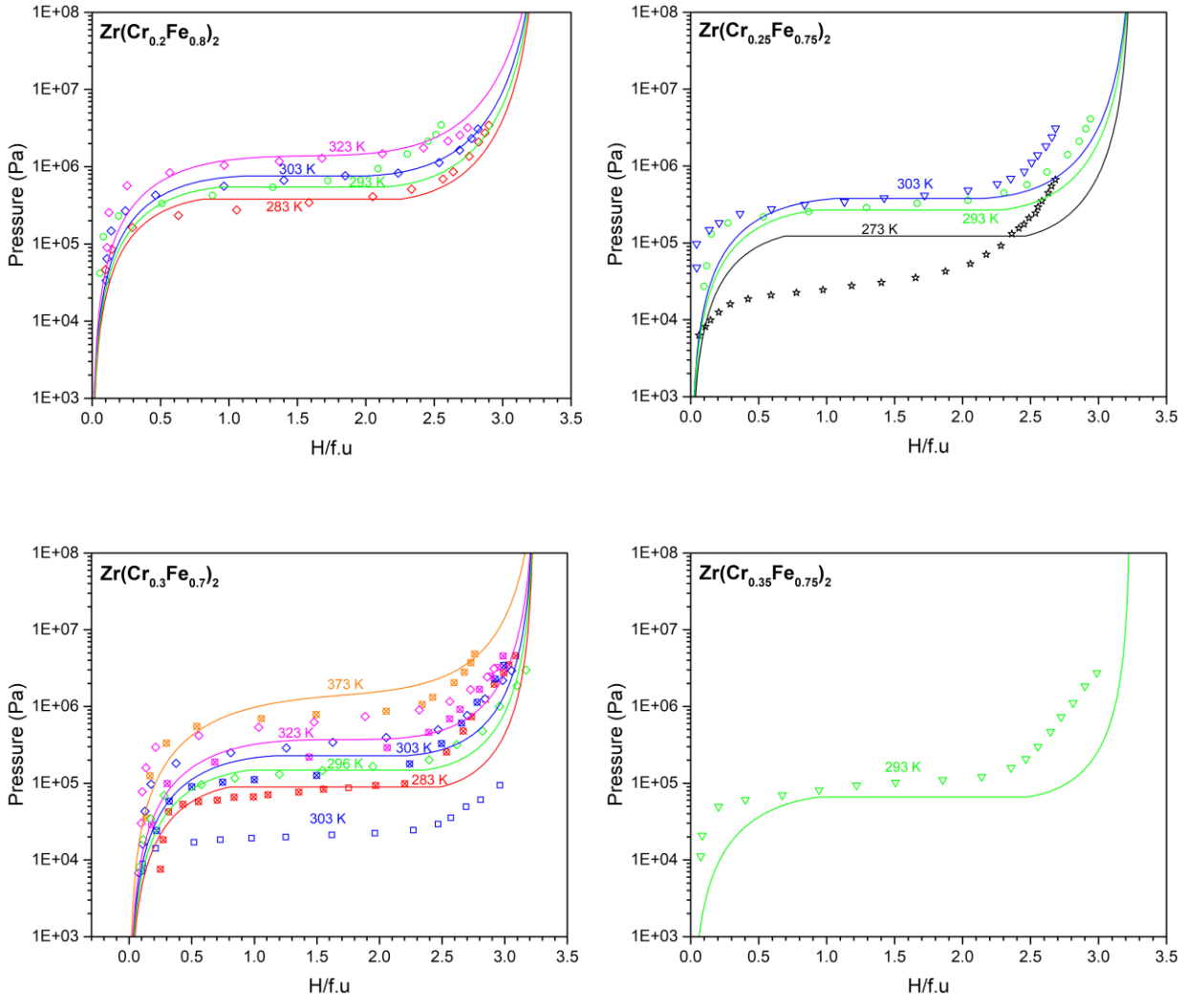

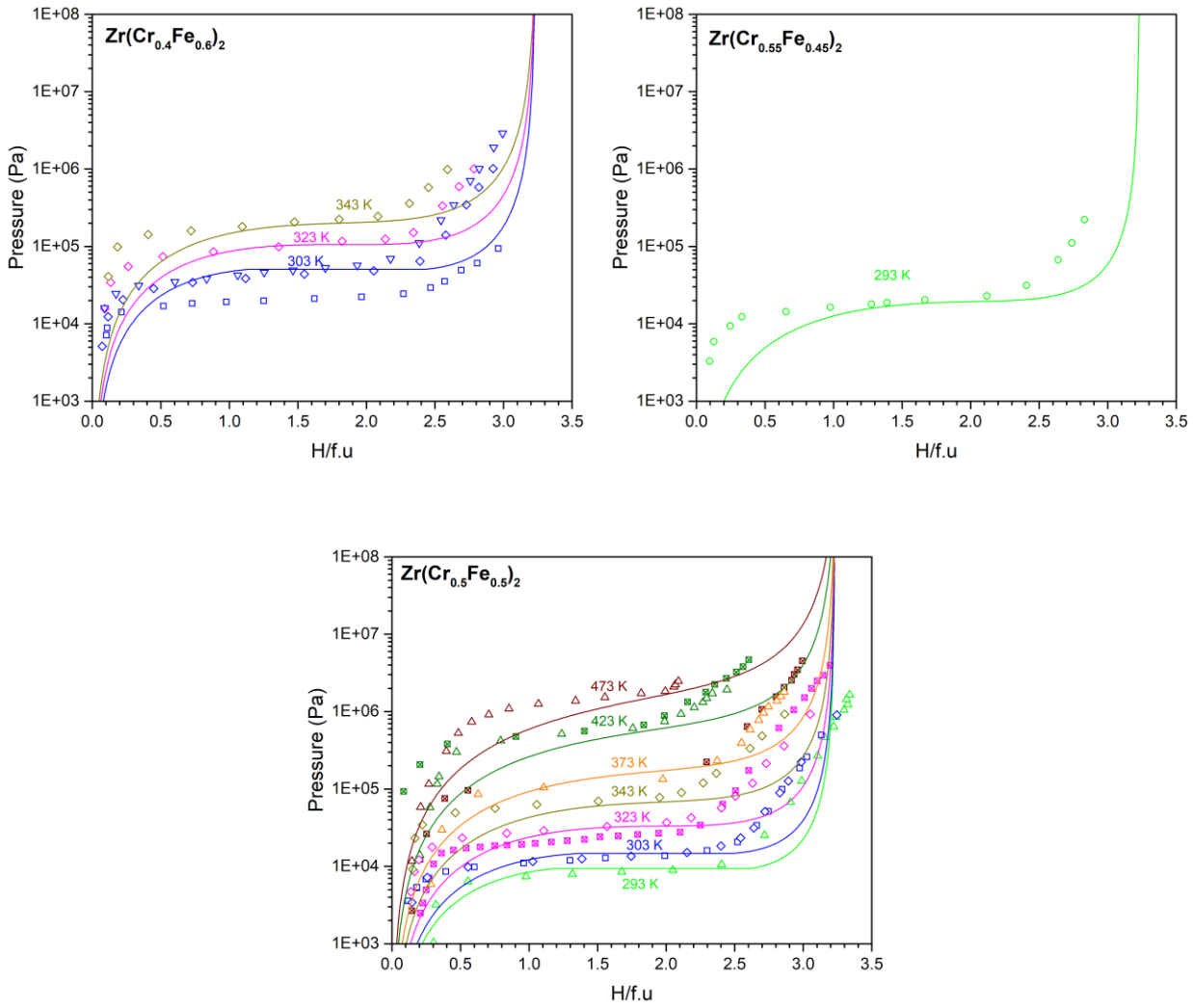

Figure 8: Calculated P-C-T diagrams of the hydride C14-$Zr(Cr_xFe_{1-x})_2$ compared with experiments: ⊠ [23], × [24], ∘ [25], △ [27], ▫ [28], ⋄ [29], ▿ [30], ⊗ [26], ⋆ [31]

The optimized diagrams (figure 8) are in acceptable agreement with the measured points. Calculated and experimental diagrams have similar behaviors: the substitution of Fe by Cr induces the decrease of the plateau pressure at a fixed temperature.

The P-C-T diagram of the *C*14-$Zr(Cr_xFe_{1-x})_2$ compound at room temperature is presented in Figure 9, along with the diagram showing the plateau pressure value for different compositions. Based on these figures, it is predicted that the composition *C*14-

$Zr(Cr_{0.32}Fe_{0.68})_2$ would be capable of absorbing hydrogen at room temperature and atmospheric pressure.

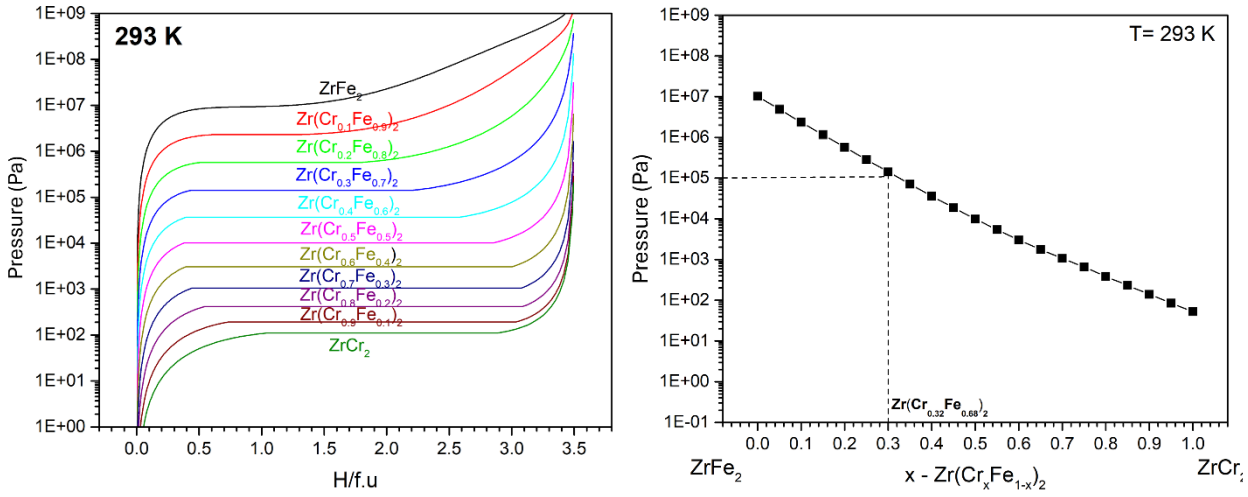

Figure 9: Plateau pressure at room temperature of the $Zr(Cr_xFe_{1-x})_2H_{3.5}$ Laves C14 hydride.

4 Conclusion

The thermodynamic assessments of Fe–H–Zr, Cr–H–Zr systems and $C14$-$Zr(Cr_xFe_{1-x})_2H_4$ hydride have been carried out. The assessments required performing the calculations in para-equilibrium conditions. According to the temperature, the paraequilibrium or the full equilibrium should be used for the calculations. An atom representing the intermetallic compositions was added in order to have the constraint of the metallic ratio for the Laves phases. This method succeeded in calculating all the hydrogenation properties of the intermetallic compounds and in reproducing the behavior of the pressure plateau while substituting Cr by Fe in the $C14$-$Zr(Cr_xFe_{1-x})_2$ compound.

Acknowledgments

The authors acknowledge Jean-Claude Crivello for the discussion on the DFT calculations. This work is funded by the projects GAINES and ICOMB within the framework of the French nuclear institute (I3P - CEA, EDF and Framatome).

Appendice: *Assessed thermodynamic parameters in this work.*

Phase	Parameters (J.mol^{-1})
BCC_A2 (Fe)(H,Va)$_3$	$G_{Fe:H}^{BCC\_A2} = +GFEH\#$ ${}^0L_{Fe:H,Va}^{BCC\_A2} = 10.83T$
HCP_A3 (Zr)(H,Va)$_2$	$G_{Zr:H:Va}^{HCP\_A3} = -91930 + 98.83T + GHSERZR\# + 2GHSERHH\#$ ${}^0L_{Zr:H,Va}^{HCP\_A3} = -3.83T$
Laves_$C15$ (Cr,Fe,Zr)$_2$(Cr,Fe,Zr)(H,Va)$_4$	$G_{Fe:Fe:H}^{Laves\_C15} = +3GHSERFE\# + 4GHSERHH\# + 10000 + 260T$ $G_{Zr:Fe:H}^{Laves\_C15} = +2GHSERZR\# + GHSERFE\# + 4GHSERHH\# +70000 + 260T$ $G_{Fe:Zr:H}^{Laves\_C15} = +2GHSERFE\# + GHSERZR\# + 4GHSERHH\# -146000 + 260T$ $G_{Zr:Zr:H}^{Laves\_C15} = +3GHSERZR\# + 4GHSERHH\# - 156000 + 260T$ $G_{Cr:Cr:H}^{Laves\_C15} = +3GHSERCR\# + 4GHSERHH\# + 144000 + 260T$ $G_{Zr:Cr:H}^{Laves\_C15} = +2GHSERZR\# + GHSERCR\# + 4GHSERHH\# +100000 + 260T$ $G_{Cr:Zr:H}^{Laves\_C15} = +2GHSERCR\# + GHSERZR\# + 4GHSERHH\# -105531.644 + 260T$ ${}^0L_{Fe:Zr:H,Va}^{Laves\_C15} = +23000$ ${}^1L_{Fe:Zr:H,Va}^{Laves\_C15} = -12000$ ${}^0L_{Cr:Zr:H,Va}^{Laves\_C15} = +25000 - 15T$

Phase	Parameters (J.mol^{-1})
Laves_$C14$ $(Cr,Fe,Zr)_4(Cr,Fe,Zr)_2(Cr,Fe,Zr)_6(H,Va)_{16}$	$G^{Laves\_C14}_{Cr:Cr:Cr:H} = +12GHSERCR\# + 16GHSERHH\# + 300000 + 1040T$ $G^{Laves\_C14}_{Zr:Cr:Cr:H} = +4GHSERZR\# + 8GHSERCR\# + 16GHSERHH\# - 478175.567 + 1040T$ $G^{Laves\_C14}_{Cr:Zr:Cr:H} = +2GHSERZR\# + 10GHSERCR\# + 16GHSERHH\# - 150000 + 1040T$ $G^{Laves\_C14}_{Zr:Zr:Cr:H} = +6GHSERZR\# + 6GHSERCR\# + 16GHSERHH\# + 1040T$ $G^{Laves\_C14}_{Cr:Cr:Zr:H} = +6GHSERZR\# + 6GHSERCR\# + 16GHSERHH\# + 1040T$ $G^{Laves\_C14}_{Zr:Cr:Zr:H} = +10GHSERZR\# + 2GHSERCR\# + 16GHSERHH\# + 1040T$ $G^{Laves\_C14}_{Cr:Zr:Zr:H} = +8GHSERZR\# + 4GHSERCR\# + 16GHSERHH\# + 400000 + 1040T$ $G^{Laves\_C14}_{Zr:Zr:Zr:H} = +12GHSERZR\# + 16GHSERHH\# - 624000 + 1040T$ $G^{Laves\_C14}_{Zr:Cr:Cr:H,Va} = +55000$
E1a $(Fe,Zr)(Fe,Zr)_3(H,Va)_7$	$G^{E1a}_{Fe:Fe:H} = +4GHSERFE\# + 7GHSERHH\# + 144226.371 + 456T$ $G^{E1a}_{Zr:Fe:H} = +GHSERZR\# + 3GHSERFE\# + 7GHSERHH\# + 75366.5123 + 456T$ $G^{E1a}_{Fe:Zr:H} = +GHSERFE\# + 3GHSERZR\# + 7GHSERHH\# - 439016.836 + 456T + 43T \times LN(T)$ $G^{E1a}_{Zr:Zr:H} = +4GHSERZR\# + 7GHSERHH\# - 328219.196 + 456T$ ${}^0L^{E1a}_{Fe:Zr:H,Va} = -80000$

Phase	Parameters (J.mol^{-1})
$C16$ $(Fe,Zr)(Fe,Zr)_2(H,Va)_5$	$G^{C16}_{Fe:Fe:H} = +3GHSERFE\# + 5GHSERHH\# + 122012.072 + 326T$ $G^{C16}_{Zr:Fe:H} = +GHSERZR\# + 2GHSERFE\# + 5GHSERHH\# +611332.481 + 326T$ $G^{C16}_{Fe:Zr:H} = +GHSERFE\# + 2GHSERZR\# + 5GHSERHH\# -325490.332 + 560T - 29.6551949TxLN(T) + 0.002T^2 + 554097.027T^{-1}$ $G^{C16}_{Zr:Zr:H} = +3GHSERZR\# + 5GHSERHH\# - 268213.481 + 326T$ ${}^0L^{C16}_{Fe:Zr:H,Va} = -100000 + 59T$

$$FUNCTIONGFEH = +213295.198 - 2916.37218T + 467.826T \times LN(T) - 0.26955T^2 + GHSERFE\# + 3GHSERHH\#; 1811Y$$

$$+241181.85 + 72.9 * T; 6000N$$

References

[1] Lafaye P, Toffolon-Masclet C, Crivello JC, Joubert JM. Experimental study, first-principles calculation and thermodynamic modelling of the Cr–Fe–Nb–Sn–Zr quinary system for application as cladding materials in nuclear reactors. Journal of Nuclear Materials 2021;544. https://doi.org/10.1016/j.jnucmat.2020.152692.

[2] Vu T-M, Gokelaere P, Toffolon-Masclet C, Joubert J-M. Thermodynamic assessment of the Fe–O–Zr, Cr–O–Zr and O–Sn–Zr ternary systems. Calphad 2025;88:102778. https://doi.org/10.1016/j.calphad.2024.102778.

[3] Krupenchenko AV, magomedbekov EP, vedernikova I. Calorimetric study of thermodynamic properties of the ZrCr2-hydrogen system. Zhurnal Fizicheskoi Khimii 1990;64:2897–908.

[4] Andreev BN, Magomedbekov EP, Sicking GH. Interaction of hydrogen isotopes with transition metals and intermetallic compounds. Berlin Heidelberg New York: Springer; 1996.

[5] Bodega J, Fernández JF, Leardini F, Ares JR, Sánchez C. Synthesis of hexagonal C14/C36 and cubic C15 ZrCr2 Laves phases and thermodynamic stability of their hydrides. Journal of Physics and Chemistry of Solids 2011;72:1334–42. https://doi.org/10.1016/j.jpcs.2011.08.004.

[6] Skripov AV, Belyaev MYu, Stepanov AP. NMR study of hydrogen mobility in C14- and C15-type compounds ZrCr2Hx. Solid State Communications 1991;78:909–12. https://doi.org/10.1016/0038-1098(91)90253-R.

[7] Pebler A, Gulbransen EA. Equilibrium studies on systems ZrCr2-H2 ZrV2-H2 and ZrMo2-H2 between 0 degrees and 900 degrees C. Transactions of the Metallurgical Society of AIME 1967;239:1593.
[8] Filipek SM, Jacob I, Paul-Boncour V, Percheron-Guegan A, Marchuk I, Mogilyanski D, et al. Investigation of ZrFe2 and ZrCo2 under very high pressure of gaseous hydrogen and deuterium. Polish Journal of Chemistry 2001;75:1921–6.
[9] Raj P, Suryanarayana P, Sathyamoorthy A, Shashikala K, Iyer RM. Zr2FeHx system hydrided at low temperatures: structural aspects by M6ssbauer and X-ray diffraction studies. Journal of Alloys and Compounds 1992;178:393–401. https://doi.org/10.1016/0925-8388(92)90280-M.
[10] S. Fukada, K. Tokunaga, M. Nishikawa. Recovery of low-concentration hydrogen from different gas streams with Zr2Fe particle beds. Fusion Engineering and Design 1997;36:471–8.
[11] Yartys VA, Fjellvåg H, Hauback BC, Riabov AB, Sørby MH. Neutron diffraction studies of Zr-containing intermetallic hydrides with ordered hydrogen sublattice. II. Orthorhombic Zr3FeD6.7 with filled Re3B-type structure. Journal of Alloys and Compounds 1998;278:252–9. https://doi.org/10.1016/S0925-8388(98)00592-1.
[12] Yartys VA, Fjellvåg H, Harris IR, Hauback BC, Riabov AB, Sørby MH, et al. Hydrogen ordering and H-induced phase transformations in Zr-based intermetallic hydrides. Journal of Alloys and Compounds 1999;293–295:74–87. https://doi.org/10.1016/S0925-8388(99)00304-7.
[13] Pitt MP, Pitt LKW, Fjellvåg H, Hauback BC. An in situ neutron diffraction study of the thermal disproportionation of the Zr2FeD5 system. Journal of Alloys and Compounds 2011;509:5515–24. https://doi.org/10.1016/j.jallcom.2011.02.129.
[14] Nobile A, Mosley WC, Holder JS, Brooks KN. Deuterium absorption and material phase characteristics of Zr2Fe. Journal of Alloys and Compounds 1994;206:83–93. https://doi.org/10.1016/0925-8388(94)90014-0.
[15] Chattaraj D, Majumder C, Dash S. Structural, electronic, elastic and thermodynamic properties of Zr 2 Fe and Zr 2 FeH 5 : A comprehensive study using first principles approach. Journal of Alloys and Compounds 2014;615:234–42. https://doi.org/10.1016/j.jallcom.2014.06.126.
[16] Zotov T, Movlaev E, Mitrokhin S, Verbetsky V. Interaction in (Ti,Sc)Fe2–H2 and (Zr,Sc)Fe2–H2 systems. Journal of Alloys and Compounds 2008;459:220–4. https://doi.org/10.1016/j.jallcom.2007.05.027.
[17] Sivov RB, Zotov TA, Verbetsky VN. Hydrogen sorption properties of ZrFex (1.9 ≤ x ≤ 2.5) alloys. International Journal of Hydrogen Energy 2011;36:1355–8. https://doi.org/10.1016/j.ijhydene.2010.06.118.
[18] Skripov AV, Karkin AE, Mirmelstein AV. Hydrogen-induced anomalies in the heat capacity of C15-type. J Phys: Condens Matter 1997;9:1191–200. https://doi.org/10.1088/0953-8984/9/6/006.
[19] Jacob I, Stern A, moran A, Shaltiel D, Davidov D. Hydrogen absorption in (Zr(x)Ti(1-x))B2 (B=Cr,Mn) and the phenomenological model for the absorption capacity in pseudo-binary Laves-Phase compounds. Journal of The Less-Common Metals 1980;73:369–76. https://doi.org/10.1016/0022-5088(80)90331-8.

[20] Hirosawa S, Pourarian F, Sinha VK, Wallace WE. MAGNETIC PROPERTIES OF Zr(Cr(1-x)Co(x))2 ALLOYS AND THEIR HYDRIDES. Journal of Magnetism and Magnetic Materials 1983;38:159–64.
[21] Canet O, Latroche M, Bourée-Vigneron F, Percheron-Guegan A. Structural study of Zr(Cr(1-x)Fe(x))2Dy (0.4<x<0.75; 2<y<3) by means of neutron powder diffraction. Journal of Alloys and Compounds 1994;210:129–34. https://doi.org/10.1016/0925-8388(94)90127-9.
[22] Soubeyroux JL, Bououdina M, Fruchart D, Pontonnier L. Phase stability and neutron diffraction studies of Laves phases Zr(Crl_xMx)2 with M=Mn, Fe, Co, Ni, Cu and 0 < x < 0 . 2 and their hydrides. Journal of Alloys and Compounds 1995;219:48–54. https://doi.org/10.1016/0022-5088(85)90368-6.
[23] Yu GY, Pourarian F, Wallace WE. The crystallographic, thermodynamic and kinetic properties of the Zr(1-x)Ti(x)CrFe-H2 system. Journal of The Less-Common Metals 1985;106:79–87. https://doi.org/10.1016/0022-5088(85)90368-6.
[24] Ivey DG, Northwood DO. Non-horizontal Plateau behaviour in Zr(Fe(x)Cr(1-x))2-H systems. Scripta Metallurgica 1985;19:1319–22. https://doi.org/0036-9748(85)90058-4.
[25] Ivey DG, Nothwood DO. Hydriding Properties of Zr(FexCrl_x)2 Intermetallic. International Journal of Hydrogen Energy 1985;11:583–91. https://doi.org/10.1016/0360-3199(86)90125-4.
[26] Wallace WE, Pourarian F. hydrogen storage materials of zirconium-chromium-iron and titanium alloys characterized by ZrCr2 stoichiometry. Journal of Alloys and Compounds 1985;105:121–7.
[27] Zhang LY, Wallace WE. Hydrogenation characteristics of the isoelectronic alloys ZrMn2, ZrCrFe, and ZrVCo. Journal of Solid State Chemistry 1988;74:132–7. https://doi.org/10.1016/0022-4596(88)90339-8.
[28] Qian S, Northwood DO. The effect of hydride formation and decomposition cycling on plateau pressures and hysteresis in Zr(Fe(x)Cr(1-x))-H systems. Journal of Materials Science Letters 1989;8:418–20. https://doi.org/10.1007/BF00720692.
[29] Qian S, Northwood DO. Thermodynamic characterization of Zr(Fe(x)Cr(1-x))2-H systems. Journal of The Less-Common Metals 1989;147:149–59. https://doi.org/10.1016/0022-5088(89)90158-6.
[30] Park JM, Lee JY. Hydrogenation characteristics of the Zr(1-x)Ti(x)Cr(1-y)Fe(1+y) Laves phase alloys. Journal of The Less-Common Metals 1990;160:259–71.
[31] Grant DM, Murray JJ, Post ML. The thermodynamics of the system Zr(Fe0.75Cr0.25)2 + H2 using heat conduction calorimetry. Journal of Solid State Chemistry 1990;87:415–22. https://doi.org/10.1016/0022-4596(90)90044-X.
[32] Lukas H, Fries SG, Sundman B. Computational thermodynamics: The Calphad method. Cambridge University Press; n.d.
[33] Pelton AD, Bale CW, Melançon J, Eriksson G, Hack K, Baben MT. Applying constraints to chemical equilibrium calculations through the use of virtual elements. Calphad 2023;81:102544. https://doi.org/10.1016/j.calphad.2023.102544.
[34] Hannappel P, Heubner F, Balcerzak M, Weißgärber T. Advancing the thermodynamic modeling of multicomponent phases in hydrogen-para-equilibrium. Acta Materialia 2025;284:120529. https://doi.org/10.1016/j.actamat.2024.120529.

[35] Joubert J-M, Thiébaut S. A thermodynamic description of the system Pd–Rh–H–D–T. Acta Materialia 2011;59:1680–91. https://doi.org/10.1016/j.actamat.2010.11.035.
[36] Matar SF, Al Alam AF, Gédéon D, Ouaini N. Changes in electronic, magnetic and bonding properties from Zr2FeH5 to Zr3FeH7 addressed from ab initio. Solid State Sciences 2013;25:55–62. https://doi.org/10.1016/j.solidstatesciences.2013.08.002.
[37] Bourgeois N. Modélisation de systèmes métal-hydrogène par couplage des méthodes DFT, CVM et Calphad. Paris-Est University, 2017.
[38] Barber CB, Dobkin DP, Huhdanpaa h. The Quickhull Algorithm for Convex Hulls. ACM Trans Math Softw 1996;22:469–83. https://doi.org/10.1145/235815.235821.
[39] Zhong Y, MacDonald DD. Thermodynamics of the Zr-H binary system related to nuclear fuel sheathing and pressure tube hydriding. Journal of Nuclear Materials 2012;423:87–92. https://doi.org/10.1016/j.jnucmat.2012.01.016.
[40] Zinkevich M, Mattern N, Handstein A, Gutfleisch O. Thermodynamics of Fe–Sm, Fe–H, and H–Sm systems and its application to the hydrogen–disproportionation–desorption–recombination (HDDR) process for the system Fe17Sm2 –H2. Journal of Alloys and Compounds 2002;339:118–39. https://doi.org/10.1016/S0925-8388(01)01990-9.
[41] Tai M, Fukayama D. Parameter Conversion of Gibbs Energy Function Between Different Sublattice Models for Interstitial Solutions. Private Communication 2016.
[42] Mohri T, Kadowaki N. Summary Report of CalphadXLV - Awaji Island, Japan. Calphad 2018:288–349. https://doi.org/10.1016/j.calphad.2017.09.001.
[43] Dottor M, Crivello J-C, Joubert J-M. Thermodynamic modeling of Cr and Cr–H systems up to high temperatures and high pressures. International Journal of Hydrogen Energy 2022;47:23293–309. https://doi.org/10.1016/j.ijhydene.2022.04.245.